Published in final edited form as:

Nat Neurosci. 2008 November ; 11(11): 1302–1310. doi:10.1038/nn.2204.

Palmitoylation-dependent neurodevelopmental deficits in a mouse model of the 22q11 microdeletion

Jun Mukai[1], **Alefiya Dhilla**[2], **Liam J. Drew**[1], **Kimberly L. Stark**[3], **Luxiang Cao**[1], **Amy B. MacDermott**[1,4], **Maria Karayiorgou**[3,^], and **Joseph A. Gogos**[1,4,^]

[1]Columbia University, College of Physicians & Surgeons, Department of Physiology and Cellular Biophysics, 630 West 168th Street, New York, NY 10032

[2]Columbia University, College of Physicians & Surgeons, Department of Pharmacology, 630 West 168th Street, New York, NY 10032

[3]Columbia University, College of Physicians & Surgeons, Department of Psychiatry, 1051 Riverside Drive, New York, NY 10032

[4]Columbia University, College of Physicians & Surgeons, Department of Neuroscience, 1051 Riverside Drive, New York, NY 10032.

SUMMARY

Individuals with 22q11.2 microdeletions have cognitive deficits and a high risk of developing schizophrenia. Here, we provide evidence that primary hippocampal neurons from a 22q11.2 deletion mouse model [*Df(16)A*$^{+/-}$] have decreased density of dendritic spines and glutamatergic synapses, as well as impaired dendritic growth. These deficits can be prevented by introduction of enzymatically active ZDHHC8 palmitoyltransferase encoded by a gene located in the 22q11.2 locus and they are also observed in primary cultures from *Zdhhc8*-deficient mice. We show that many of these deficits are also present in the hippocampus of adult *Df(16)A*$^{+/-}$ and *Zdhhc8*-deficient mice. Finally, we provide evidence that PSD95 is one of the substrates of ZDHHC8. Our analysis reveals that 22q11.2 microdeletion results in deficits in neuronal development and suggests that impaired neuronal protein palmitoylation contributes to many of these deficits.

INTRODUCTION

Microdeletions of the 22q11.2 locus are among the most common chromosomal abnormalities and occur predominantly *de novo*1. Children with the 22q11.2 microdeletion show high incidence of emotional problems2, exhibit a spectrum of cognitive deficits2,3,4 and ~30% of them develop schizophrenia or schizoaffective disorder in adolescence or early adulthood5,6. Recurrent 22q11.2 microdeletions account for up to 1–2% of sporadic schizophrenia cases7,8.

^Correspondence should be addressed to M.K. (mk2758@columbia.edu) and J.A.G. (jag90@columbia.edu).

AUTHOR CONTRIBUTIONS

JM, AD, LJD and LC performed research; KLS contributed reagents; JM, AD, LJD, ABM analyzed data; MK and JAG supervised the project and JM, AD, LJD, ABM, MK and JAG wrote the paper.

The majority of patients have a hemizygous 3-Mb deletion, while 7% have a nested 1.5-Mb deletion encompassing an area containing 27 known genes9. Genetic analysis has provided important insights into the genetic basis of the psychiatric and cognitive symptoms observed in adult 22q11.2 microdeletion carriers and implicated a subset of these genes10–13. Among them, *ZDHHC8* is a putative palmitoyl-transferase (PAT), which belongs to a 23-member family of enzymes that share a conserved cysteine-rich signature catalytic domain (DHHC domain)14–17. Protein palmitoylation involves the attachment of the 16-carbon saturated fatty acid palmitate to specific cysteine residues and has emerged as a key reversible post-translational protein modification. It is involved in the regulation of protein trafficking and the functional modulation of diverse membrane and cytosolic proteins, especially in neurons18,19. Interestingly, in addition to the hemizygous deletion of the *ZDHHC8* gene in 22q11 microdeletion carriers, a genetic variant of *ZDHHC8*, which modulates the relatively complex pattern of splicing of the gene, was shown to be associated with schizophrenia in several, but not all, tested cohorts of karyotypically normal patients11,20,21 (see also Suppl. Note).

The orthologous region of the human 22q11.2 locus lies on mouse chromosome 16. With the exception of one gene, all of the functional human genes in this region are represented in the mouse, although organized in a slightly different order22. By using chromosomal engineering, we generated a mouse model carrying a 1.3-Mb chromosomal deficiency (*Df(16)A*), which is syntenic to the 22q11.2 1.5-Mb microdeletion [$Df(16)A^{+/-}$ mice]23. In addition, we have previously reported the generation and initial characterization of a mouse strain carrying a deletion of the *Zdhhc8* gene11. $Df(16)A^{+/-}$ and *Zdhhc8*-deficient mice do not show gross brain abnormalities and present a partially overlapping pattern of cognitive and affective behavioral deficits (ref. 11, 23 and unpublished data).

Here, we present results of a comprehensive analysis of hippocampal pyramidal neurons from both of these mouse models. We provide evidence that primary hippocampal neurons from $Df(16)A^{+/-}$ mice have a decreased density of dendritic spines and glutamatergic synapses, as well as impaired dendritic growth, both of which can be prevented by re-introduction of enzymatically active ZDHHC8 protein. We also show similar alterations in hippocampal neurons from *Zdhhc8*-deficient mice. Many of the deficits we observe in primary cultures are also observed in the hippocampus (HPC) of adult $Df(16)A^{+/-}$ and *Zdhhc8*-deficient mice. Finally, we show that ZDHHC8 can palmitoylate postsynaptic density-95 (PSD95), an adaptor molecule known to modulate the number of dendritic spines24,25 and possibly dendritic branches26. The palmitoylation-dependent structural and functional changes we describe represent possible predisposing factors to the psychiatric and cognitive symptoms associated with the 22q11.2 microdeletion.

RESULTS

22q11.2 microdeletion affects dendritic spine density

The impact of the 22q11.2 microdeletion on neuronal development remains unknown. To examine first whether *Df(16)A* (Fig. 1a) affects the density and morphology of dendritic spines, we transfected conventional mass hippocampal neuronal cultures with constructs encoding GFP and viewed the spine morphology27 of GFP-positive pyramidal neurons

using confocal imaging at DIV21. Analysis of dendritic spine development showed that mushroom spine density was reduced in *Df(16)A*$^{+/-}$ neurons at DIV21 (46%, $n = 13$, $P < 0.0001$) compared to wild-type (WT) neurons ($n = 12$) (Fig. 1b,c), while the density of other spine morphotypes and filopodia was not significantly affected (see Suppl. Fig. 1a). Morphometric analysis of mushroom spines showed a small, but statistically significant decrease in the head-width and length (Fig. 1d). The average spine head-width was decreased by 23% in *Df(16)A*$^{+/-}$ neurons ($n = 176$, $P < 0.0001$) and the average length was decreased by 18.5% ($n = 176$, $P < 0.0001$) compared to WT neurons ($n = 267$). Dendritic spines represent the postsynaptic compartment for the majority of glutamatergic synapses. To test whether the decrease in spine numbers is accompanied by a decrease in glutamatergic synapses we recorded miniature excitatory postsynaptic currents (mEPSCs) in hippocampal neurons collected from *Df(16)A*$^{+/-}$ mice, as well as from their WT littermates. Individual neurons were grown on microislands of astrocytes28 and synaptic activity was recorded 11 – 14 days after plating. In the *Df(16)A*$^{+/-}$ neurons, mEPSCs occurred at significantly lower frequencies (1.18 ± 0.36 Hz, $n = 10$) than in WT neurons (3.33 ± 0.78 Hz, $n = 11$, $P < 0.05$, Fig. 1e). Conversely, neither the amplitude (*Df(16)A*$^{+/-}$: 14.10 ± 1.72 pA, WT: 13.36 ± 1.29 pA) (Fig. 1e) nor the kinetics (data not shown) of the synaptic events were altered by the deletion. These data are consistent with the decrease in the number of spines and suggest that glutamatergic synapses are established at a lower density although functional synapses display normal quantal amplitudes.

To further confirm the reduction in the density of glutamatergic synapses, we used quantitative immunocytochemistry (ICC) in combination with confocal microscopy to evaluate the density of a) clusters of PSD95, an adaptor protein involved in clustering postsynaptic receptors at glutamatergic synapses29,30 and b) clusters of vesicular glutamate transporter-1 (VGLUT1), specific to glutamatergic neurons for loading glutamate into synaptic vesicles, as a presynaptic marker31. We found that *Df(16)A* results in a reduction in the density of both markers. Specifically, the density of clusters of PSD95 at DIV21 was reduced (47%, $P < 0.0001$) in *Df(16)A*$^{+/-}$ mice ($n = 18$) compared to their WT littermates ($n = 18$) (Fig. 1f,g). This reduction in the density of PSD95 puncta was also evident in younger (DIV9) *Df(16)A*$^{+/-}$ neurons (47%, $P < 0.001$, $n = 24$) compared to WT neurons ($n = 24$) (Fig. 1g). The density of VGLUT1 clusters in neurons from *Df(16)A*$^{+/-}$ mice was also reduced at DIV21 (34%, $n = 21$, $P < 0.0001$) compared to their WT littermates ($n = 21$) (Fig. 1f,h). This reduction in the density of VGLUT1 puncta was also evident in younger (DIV12) neurons (56%, $P < 0.0001$; $n = 33$) compared to WT neurons ($n = 24$) (Fig. 1h). Evaluation of the density of additional postsynaptic markers Homer1 (an adaptor protein enriched in glutamatergic synapses25) and GluR2 (an AMPA receptor subunit), corroborated the reduced density of excitatory postsynaptic complexes (see Suppl. Fig. 2a,b). It should be noted that at DIV21 the majority of PSD95, Homer1 and GluR2 puncta (81.0%, 92.5%, 89.2%, respectively, in the WT neurons) are located at synaptic sites (that is they overlap with synaptophysin, a presynaptic marker, or VGLUT1). As expected, the density of clusters of postsynaptic markers is reduced when only synaptic puncta are considered (data not shown).

Zdhhc8-deficiency affects dendritic spine density

An increasing number of molecules, several of them substrates for palmitoylation, are known to regulate the formation and maturation of dendritic spines and glutamatergic synapses. Therefore, we considered the possibility that reduction in the density of spines and excitatory contacts emerging as a result of *Df(16)A* may be, at least in part, due to removal of one copy of the mouse *Zdhhc8* gene. The gene is expressed in both HPC and cortex11 and is localized primarily in the Golgi apparatus and the vesicular compartment11,32.

We first transfected *Df(16)A*$^{+/-}$ neurons with a full-length *ZDHHC8* construct (henceforth referred to as *ZDHHC8-FL*). Expression of *ZDHHC8-FL* was able to restore the number of mushroom spines to nearly WT levels. By contrast, *Df(16)A*$^{+/-}$ neurons transfected with a construct carrying a mutation in the critical cysteine 134 in the DHHC domain to an alanine (*ZDHHC8-C134A* form), which is known to block PAT activity16, maintained reduced numbers of mushroom spines (Fig. 2a,b and Suppl. Fig. 1a). Notably, neither the transfection of *ZDHHC8-FL* nor of *-C134A* in *Df(16)A*$^{+/-}$ neurons influenced spine width or length ($P > 0.05$, Kolmogorov-Smirnov (K-S) test, Fig. 2c). To elucidate whether ZDHHC8 activity can also reverse the deficit in the density of pre- and postsynaptic marker clusters, we transfected *ZDHHC8-FL* or *-C134A* forms into *Df(16)A*$^{+/-}$ neurons. Expression of ZDHHC8-FL, but not of the -C134A, restored the number of PSD95, VGLUT1, Homer1 and GluR2 puncta to WT levels (Fig. 2d,e and Suppl. Fig. 2c,d).

We then collected primary neurons from homozygous and heterozygous knockout mice that lacked the gene encoding Zdhhc8 (*Zdhhc8*$^{-/-}$ and *Zdhhc8*$^{+/-}$), as well as their WT (*Zdhhc8*$^{+/+}$) littermates11. We found that compared to neurons from WT mice ($n = 12$), the number of mushroom spines (but not other spine morphotypes or filopodia) in *Zdhhc8*$^{+/-}$ and *Zdhhc8−/−* neurons were reduced by 40% ($n = 12$, $P < 0.0001$) and 43($n = 12$, $P < 0.0001$), respectively (Fig. 3a,b and Suppl. Fig. 1b). However, consistent with the observation that increase in ZDHHC8 activity fails to rescue deficits in spine width or length of *Df(16)A*$^{+/-}$ neurons, we found that *Zdhhc8*-deficiency did not affect the width or length of mushroom spines (Fig. 3c).

We also observed a reduction in the density of glutamategic synaptic contacts. In mature neurons (DIV21), the density of PSD95 puncta was reduced by about 46% ($P < 0.0001$) in both *Zdhhc8*$^{+/-}$ ($n = 32$) and *Zdhhc8−/−* ($n = 18$) neurons compared to PSD95 puncta in WT neurons ($n = 18$) (Fig. 3d,e). Similar to *Df(16)A*$^{+/-}$ mice, this reduction in the density of PSD95 puncta was also evident in younger (DIV9) neurons: reduction by 16.5% in *Zdhhc8*$^{+/-}$ neurons ($n = 18$, $P < 0.1$) and by 29% in *Zdhhc8−/−* neurons ($n = 18$, $P < 0.05$) compared to WT neurons ($n = 18$) (Fig. 3e). In mature neurons (DIV21), the density of VGLUT1 puncta was reduced by about 35% ($P < 0.001$) in *Zdhhc8*$^{+/-}$ ($n = 21$) and by 39.5% in *Zdhhc8−/−* neurons ($n = 21$, $P < 0.0001$) neurons compared to VGLUT1 puncta in WT neurons ($n = 21$) (Fig. 3d,f). This reduction was also evident in younger (DIV12) neurons: (24% in *Zdhhc8*$^{+/-}$ ($n = 30$, $P < 0.05$) and by 58% in *Zdhhc8*$^{-/-}$ neurons ($n = 28$, $P < 0.0001$) compared to WT neurons ($n = 24$) (Fig. 3f). Evaluation of the density of Homer1 and GluR2 puncta corroborated the reduced density of excitatory complexes (Suppl. Fig. 2e,f). In control experiments, we confirmed that the observed reduction in spine density and

number of excitatory synaptic contacts is a direct effect of reduced Zdhhc8 PAT activity (see Suppl. Data, Suppl. Figs. 1b and 3).

Zdhhc8-deficiency affects dendritic complexity

We also examined whether *Df(16)A* affects dendritic complexity. We transfected dissociated hippocampal neurons at DIV7 with constructs encoding EGFP in order to visualize their morphology (Fig. 4a). Thirty-six hours after transfection (DIV9), we fixed and stained the transfected hippocampal neurons with a MAP2 antibody to identify dendrites. An analysis of dendritic complexity revealed a decrease in the number of primary dendrites, number of branchpoints, and total length of MAP2 stained dendrites from *Df(16)A*$^{+/-}$ mice (Fig. 4a). Specifically, *Df(16)A*$^{+/-}$ neurons (n = 19) showed a decrease in the number of branchpoints (45%, $P < 0.01$ at DIV9) (Fig. 4b), as well as in the number of primary dendrites (38%, $P < 0.0001$ at DIV9) (Fig. 4c) compared to WT neurons (n = 16). Thus, hemizygous deletion of the mouse equivalent of the human 1.5-Mb 22q11.2 locus results in reduced dendritic complexity in primary cultured neurons.

Previous evidence suggests that palmitoylation may affect dendritogenesis33. Therefore, we asked whether ZDHHC8 PAT activity contributes to the observed deficits in dendritic complexity in the *Df(16)A*$^{+/-}$ neurons. First, we expressed *ZDHHC8-FL* and the enzymatically inactive -*C134A* form in hippocampal neurons from *Df(16)A*$^{+/-}$ mice. We found that in *Df(16)A*$^{+/-}$ neurons expressing *ZDHHC8-FL* the number of total branchpoints and primary dendrites were restored to normal WT levels, while the enzymatically inactive -*C134A* form did not influence these parameters (Fig. 4a,d,e). Second, we analyzed dendritic morphogenesis in primary hippocampal neurons collected from *Zdhhc8*−/− and *Zdhhc8*$^{+/-}$ mice, as well as their WT (*Zdhhc8*$^{+/+}$) littermates. We found that the pattern and degree of dendritic arbor simplification were very similar to the ones observed in *Df(16)A*$^{+/-}$ neurons. Specifically, we found that *Zdhhc8* deficiency caused a decrease in the number of branchpoints in the *Zdhhc8*$^{+/-}$ (37%, n = 20, $P < 0.0001$), as well as in the *Zdhhc8*$^{-/-}$ neurons (41%, n = 30, $P < 0.0001$), compared to WT neurons (n = 24) (Fig. 4f,g). The number of primary dendrites was also reduced by 12% in the *Zdhhc8*$^{+/-}$ (n = 20, $P < 0.05$) and by 19.5% in the *Zdhhc8*−/− neurons (n = 19, $P < 0.001$) compared to WT neurons (n = 18) (Fig. 4h). We confirmed that the reduction in dendritic complexity is a direct effect of reduced Zdhhc8 PAT activity (see Suppl. Data and Suppl. Fig. 4).

Morphological alterations in the HPC of mutant mice

We examined whether deficits observed *in vitro* in neuronal cultures are recapitulated in the HPC of adult mice. We intercrossed *Df(16)A*$^{+/-}$ mice and *Zdhhc8*-deficient mice with a reporter strain (Thy-1-GFP/M line) where CA1 neurons are labeled in a mosaic manner with GFP34 allowing visualization of the dendritic arbors and spines. We observed a reduction in the mushroom spine density (albeit less pronounced than the one observed in cultured neurons) in CA1 pyramidal neurons from *Df(16)A*$^{+/-}$ mice (n = 20) compared to WT mice (n = 18) (24%, $P < 0.001$) (Fig. 5a,b). The density of other spine morphotypes was not affected (see Suppl. Fig. 1c). In addition, similar to the cultured *Df(16)A*$^{+/-}$ neurons there was a significant but lower-magnitude decrease in the spine width of CA1 pyramidal neurons (Fig. 5c). The average head-width was decreased by 10.7% in spines of *Df(16)A*$^{+/-}$

CA1 neurons (n = 524) compared to WT CA1 neurons (n = 608) ($P < 0.0001$). By contrast, we did not observe any changes in spine length.

To examine whether the decrease in spine density is accompanied by a decrease in the density of glutamatergic synapses *in vivo*, we used quantitative immunohistochemistry (IHC), to measure the number of PSD95 and VGLUT1 puncta in both apical (SR: stratum radiatum) and basal (SO: stratum oriens) dendrites of pyramidal cells sampled along the dorsal/ventral axis of CA1. We found a significant reduction in the number of puncta in both layers in the *Df(16)A*$^{+/-}$ mice [PSD95: SO: 23%, n = 45, $P < 0.0001$; SR: 11%, n = 45, $P < 0.001$ / VGLUT1: SO: 20%, n = 36, $P < 0.0001$; SR: 15.3%, n = 40, $P < 0.0001$) (Fig. 5d–f and data not shown). Notably, the amount of total PSD95 and VGLUT1 protein was also reduced in hippocampal lysates from 8-week old *Df(16)A*$^{+/-}$ mice (28.5%, n = 4, $P < 0.05$ and 24.9%, n = 7, $P < 0.05$, respectively) compared to WT littermates (Fig. 5g). A decrease in PSD95 levels was also observed in the PSD-enriched (Triton X-100 insoluble) fraction of HPC (see Suppl. Fig. 5).

In further support of the notion that loss of one copy of the *Zdhhc8* gene contributes to the deficits in the density of dendritic spines and synaptic markers observed in the HPC of *Df(16)A*$^{+/-}$ mice, we found a similar gene-dosage dependent pattern of deficits in the HPC of *Zdhhc8*-deficient mice. Specifically, the significant reduction in mushroom spine density observed in *Zdhhc8*-deficient primary hippocampal neurons was also observed *in vivo* in CA1 pyramidal neurons from adult *Zdhhc8*$^{+/-}$ (n = 12) and *Zdhhc8*$^{-/-}$ (n = 12) mice when compared to WT mice (n = 12) (Fig. 5h,i and Suppl. Fig. 1d), although again the level of reduction was less pronounced (16%, $P < 0.05$, and 23%, $P < 0.001$, respectively). A morphotypic analysis of mushroom spines showed that, similar to cultured *Zdhhc8*$^{+/-}$ and *Zdhhc8*−/− neurons, there were no significant changes in the width and length of CA1 pyramidal spines (Fig. 5j).

Furthermore, quantification of puncta in both the SO and SR layers in *Zdhhc8*$^{+/-}$ and *Zdhhc8*−/− mice and their WT littermates indicated a significant reduction in the number of PSD95 puncta in both layers in the *Zdhhc8*$^{+/-}$ mice (SO: 17%, n = 15, $P < 0.01$; SR: 19.5%, n = 17, $P < 0.001$) and in the *Zdhhc8*−/− mice (SO: 24%, n = 14, $P < 0.0001$; SR: 27%, n = 14, $P < 0.001$) (Fig. 5k,l and data not shown). The same analysis also indicated significant reduction in the number of VGLUT1 puncta in both layers in the *Zdhhc8*$^{+/-}$ mice (SO: 16%, n = 45, $P < 0.0001$; SR: 16%, n = 45, $P < 0.0001$) and in the *Zdhhc8*−/− mice (SO: 21%, n = 45, $P < 0.0001$; SR: 22%, n = 45, $P < 0.0001$) (Fig. 5k,m and data not shown). In addition to the reduction in the number of puncta, the amount of total PSD95 and VGLUT1 protein was reduced in hippocampal lysates from 8-week old mutant mice: *Zdhhc8*$^{+/-}$ (26%, n = 4, $P < 0.05$ and 8.2%, n = 7, $P < 0.05$, respectively) and *Zdhhc8*$^{-/-}$ (39%, n = 4, $P < 0.05$ and 26.8%, n = 7, $P < 0.0001$, respectively) (Fig. 5n). A decrease in the PSD95 levels was also observed in the PSD-enriched (Triton X-100 insoluble) fraction of HPC (see Suppl. Fig. 5).

Finally, consistent with the results obtained in culture, we observed a simplification of the dendritic complexity of CA1 pyramidal neurons in *Df(16)A*$^{+/-}$*;Thy1-GFP*$^{+/-}$ mice (Fig. 6a–c). Eight-week old *Df(16)A*$^{+/-}$*;Thy1-GFP*$^{+/-}$ mice show a decrease in the number of branchpoints in the basal dendritic tree of CA1 neurons (25%, n = 17, $P < 0.05$) compared to

WT *Thy1-GFP*$^{+/-}$ (n = 17) (Fig. 6b). This finding was confirmed by a Sholl analysis, which indicated a genotype effect when comparing branchpoint numbers at varying distances from the soma (n = 35, $P < 0.01$) (Fig. 6c).

Analysis of CA1 pyramidal neurons in *Zdhhc8*$^{+/-}$ and *Zdhhc8*$^{-/-}$ mice also showed a simplification in the dendritic arbors (Fig. 6d–f). Specifically, we found that 8-week old *Zdhhc8*$^{+/-}$ and *Zdhhc8*$^{-/-}$ mice show a decrease in the total number of branchpoints in the basal dendritic tree of CA1 neurons (19%, n = 9, $P < 0.05$ and 21%, n = 9, $P < 0.01$) compared to *Zdhhc8*$^{+/+}$*;Thy1-GFP*$^{+/-}$ (n = 12) (Fig. 6e). This finding was confirmed by a Sholl analysis, which indicated a genotype effect in a repeated measures ANOVA comparing branchpoint numbers at varying distances from the soma (*Zdhhc8*$^{+/+}$, n = 12; *Zdhhc8*$^{+/-}$, n = 9; *Zdhhc8*$^{-/-}$, n = 9, $P < 0.001$) (Fig. 6f).

ZDHHC8 modulates PSD95 palmitoylation

A large number of molecules can regulate formation of dendritic spines and branches and the assembly of postsynaptic elements35,36. Several of these molecules are substrates for palmitoylation and potential ZDHHC8 substrates. Postsynaptic density proteins, such as PSD95 or PSD93 [members of the membrane associated guanylate kinase (MAGUK) superfamily], are good candidates to contribute to the observed phenotypes for two reasons: first, they represent a large fraction of the palmitoylated proteins in brain19,37,38; second, previous work has demonstrated that manipulation of endogenous PSD95 levels modulates the number of dendritic spines24,25,39, and possibly dendritic branches26. To test whether ZDHHC8 shows PAT activity toward PSD95 or PSD93, we used heterologous HEK293 cells to co-express full-length *ZDHHC8-FL* with PSD95 or PSD93, as well as with other palmitoylated neuronal proteins, including GAP43, SNAP25, GAD65 and Synaptotagmin-133,40–43. We monitored palmitoylation by metabolic labeling with [^{3}H] palmitate, a radioactive precursor that is incorporated faithfully into palmitoylated proteins44. Transfected *ZDHHC8-FL* increased the amount of radiolabeled palmitate incorporated by PSD95 in a dose-dependent manner (Fig. 7a). It also increased incorporation by PSD93 (Suppl. Fig. 6) and GAP43 (not shown), but showed weak or no enzymatic activity toward palmitoylation of SNAP25, GAD65 and Synaptotagmin-1 (Fig. 7b). Thus, as expected, ZDHHC8 appears to be involved in the palmitoylation of a specific subset of neuronal proteins with a more pronounced effect on PSD95.

PSD95 is dually palmitoylated at cysteine residues 3 and 519,38 and, as expected, mutation of PSD95 cysteines 3 and 5 to serines (PSD95C3,5S) abolished palmitoylation in our metabolic labeling assay (Fig. 7a). We also found that mutating the critical cysteine 134 in the DHHC domain to an alanine (ZDHHC8-C134A form) blocked PSD95 palmitoylation, consistent with the role of the DHHC domain in PAT activity16 (Fig. 7a). Finally, we confirmed the results from the metabolic labeling assays using two additional *in vitro* surrogate assays for palmitoylation, which are based on the observation that in heterologous HEK293 cells palmitoylation affects both the trafficking of PSD95 (resulting in accumulation in a perinuclear domain) and its association with cellular membranes14,45. Specifically, we showed that co-transfection with *ZDHHC8-FL* resulted in re-distribution of PSD95 from the cytoplasm to a perinuclear region (Fig. 7c, *left*). This re-distribution

requires an intact DHHC domain of ZDHHC8 (Fig. 7c, *left*), as well as the critical cysteines of PSD95 since transfected PSD95C3,5S, which is not palmitoylated, localizes diffusely throughout the cytoplasm even in the presence of ZDHHC8 (data not shown). Moreover, while at steady-state PSD95 can be found in both the Triton X-100-soluble (*C*) and the Triton X-100-insoluble (*M*) fractions of lysates from transfected HEK293 cells, co-transfection with *ZDHHC8-FL* causes a re-distribution of WT PSD95 to the Triton X-100-insoluble fraction, which is enriched in membrane-associated proteins (Fig. 7c, *right*). This effect depends on both the critical cysteines of PSD95 (data not shown) and requires the DHHC domain (Fig. 7c, *right*).

We then asked whether *Zdhhc8*-deficiency affects palmitoylation of endogenous PSD95 in primary hippocampal neurons collected from homozygous knockout mice (*Zdhhc8*$^{-/-}$). We found that the incorporation of [^{3}H] palmitate by PSD95 in *Zdhhc8*$^{-/-}$ neurons was reduced by 45% compared to the WT neurons ($n = 10$, $P < 0.0001$) following 180 minutes of incubation with [^{3}H] palmitate (Fig. 7d).

DISCUSSION

Our work here provides the first evidence that the 22q11.2 microdeletion results in deficits in synaptic connectivity and neuronal morphology and strongly suggests that *Zdhhc8*-deficiency contributes, at least in part, to many of these deficits. Specifically, our findings reinforce the notion that ZDHHC8 is critical for establishing normal levels of mushroom spines, but also reveal additional non-*Zdhhc8* dependent deficits in spine morphogenesis in neurons carrying a deletion of the orthologous 22q11.2 locus. We have recently shown that the observed decreases in the size of the dendritic spines observed *in vivo* in *Df(16)A*$^{+/-}$ mice are related, at least in part, to abnormal brain microRNA biogenesis in these mice due to loss of one copy of the *Dgcr8* gene23. Contributions from more than one gene to the morphological phenotypes described in this study are consistent with genetic work suggesting an oligogenic basis for the psychiatric and cognitive symptoms associated with 22q11.2 microdeletions12,46.

The concordance of our analysis in dissociated cultures and the intact animal is extensive, although qualitative and quantitative differences were also observed. Whether effects unmasked in primary culture neurons are also observed at the level of the organism depends on network level influences that cannot be recapitulated in dissociated cultured neurons, as well as on the emergence of developmental compensations due to changes in gene expression or activity. Indeed, large scale expression profiling of the HPC of *Df(16)A*$^{+/-}$ mice23 revealed changes in the expression of clusters of genes modulating synaptic transmission, including transcript upregulation of PSD95 and of several genes that functionally and physically interact with it at glutamatergic synapses. In addition, it is possible that other DHHC family members that share redundant function and are expressed during the life of the organism could partly compensate for the effects observed in neuronal cultures.

The mechanistic basis of the observed effects remains to be elucidated and awaits identification of *bone fide* substrates of ZDHHC8. Along these lines, we found that

ZDHHC8 can palmitoylate PSD95, an adaptor molecule previously shown to modulate the number of dendritic spines24,25 and possibly dendritic branches26. Thus, reduced palmitoylation of PSD95 could contribute to the 22q11.2-associated neurodevelopmental deficits. Such interpretation is consistent with the observation that reduction in the density of clusters of postsynaptic markers appears early in the development of cultured pyramidal neurons and predates the emergence of deficits in dendritic spines. Interestingly, we also found a reduction in the levels of total PSD95 in the HPC of both *Zdhhc8*-deficient and *Df(16)A*$^{+/-}$ mice. This reduction could indicate a direct or indirect effect of palmitoylation on PSD95 stability as it has been shown for other palmitoylated proteins47. It should be noted, however, that each member of the DHHC family of PATs is predicted to have multiple substrates14,48 and therefore it is very likely that the observed phenotypes are due to combined under-palmitoylation of additional substrates, which remain to be identified (JM, MK, JAG unpublished data). In addition, other members of the DHHC family were previously shown to palmitoylate PSD95 in cultured neurons14,48 and the presence of additional PSD95 PATs is supported by our data showing that PSD95 palmitoylation is not abolished in *Zdhhc8*$^{-/-}$ mice.

In considering the implications of the findings of this and other related studies it is tempting to speculate that the altered neuronal development and connectivity that emerges due to deficits in neuronal palmitoylation and likely microRNA biogenesis23 contribute to the behavioral, cognitive and information-processing deficits associated with the 22q11 microdeletion. In that context, a superimposed abnormal neuromodulatory function in dopamine neurotransmission brought on by the previously demonstrated combined deficiency in two other genes in this locus12,13 could further alter network properties, modify the cognitive phenotypes and possibly predispose a subset of 22q11 microdeletions carriers to psychiatric symptoms. In this model, decreases in the dosage of neighboring genes would have a cumulative effect on the properties of neural networks resulting in a continuum of neuronal dysconnectivity and aberrant neuromodulation, which lead to a disease state when a critical threshold of dysfunction is surpassed. How the genetic pathways characterized so far interact at the circuit and neural systems levels49 to modulate the input/output function of specific brain areas remains unknown. Deciphering these interactions will provide valuable mechanistic insights into the pattern and severity of the 22q11.2-associated cognitive and psychiatric symptoms.

METHODS

Zdhhc8-deficient and *Df(16)A*$^{+/-}$ transgenic mice

Generation of these mouse strains has been described in detail previously in refs. 11 and 23 (See also Suppl. Methods and Suppl. Fig. 7). All animal procedures were conducted according to protocols approved by the Institutional Animal Care and Use Committee established by Columbia University under federal and state regulations.

Expression Constructs, Antibodies and conditions used for ICC and IHC, Cell culture and transfection, Metabolic labeling and Subcellular fractionation are described in detail in Suppl. Methods.

Image acquisition and quantification

Image acquisition is described in detail in Suppl. Methods.

Image analysis of puncta number

Image analysis was performed blind to the genotype as follows:

In vitro—The number of fluorescent puncta were quantitated using confocal images at maximum projection within a region of interest (ROI) encompassing a 50 μm region proximal to the soma in one or two of the largest dendrites in each neuron. ImageJ software was used to count the number of fluorescent puncta. The particle measurement feature was utilized to count the number of discrete puncta of the image. All settings of minimal puncta size and threshold were maintained constant across genotypes. Puncta numbers were compared across genotypes from 3 independent experiments using a Student's *t*-test.

In vivo—The number and intensity of puncta were examined in the SO and the SR subfields of the CA1 region of the HPC, which contain the basal dendrites and the apical dendrites of pyramidal cells, respectively. Data was analyzed by counting the number of puncta in a sampling of 5 consecutive optical sections in the stack. The ROI in the SO and SR was defined by a 71.4 μm×64.2 μm box. The particle measurement feature was then utilized, with a same setting of minimal puncta size and threshold, to count the number of discrete puncta of the image. Puncta number were first averaged across optical sections and then compared statistically across regions of the HPC, as well as genotype, using ANOVA.

Image analysis of dendritic complexity

Image analysis was performed blind to the genotype as follows:

In vitro—A plasmid expressing GFP driven by the β-actin promoter was transfected into cultures in order to fill the cells and facilitate visualization of all processes. *Z*-stacks were projected maximally and neuronal processes stained for the dendritic marker MAP2 were traced using the overlay tools of the LSM Image Examiner 5 program. Protrusions more than 8 μm were categorized as dendrites. Once the elaborations of the dendritic tree had been outlined, the number of branchpoints and the number of primary dendrites (emanating directly from the soma) were counted manually and compared statistically across three independent experiments using a Student's *t*-test.

In vivo—The complexity of the basal dendrites of CA1 neurons in *Thy1-GFP*$^{+/-}$ mice was analyzed by projecting the *z*-series to maximum intensity and manually tracing the dendritic tree. Sholl analysis was conducted using concentric radii of 10 μm extending from the center of the soma. Intersections, branches, and terminals were counted by distance from the soma, and the statistical significance of differences was measured by repeated-measures ANOVA. The internal architecture of each neuron was also characterized by designating the order of a process (primary, secondary, etc.) and whether it branched (segment) or not (terminal). The number and average lengths of all process types were compared between mutant and WT neurons (17 neurons from 5 animals of each genotype) using a repeated-measures ANOVA test.

Image analysis of dendritic spines

Image analysis was performed blind to the genotype as follows:

In vitro—Spine density and morphology measurements were conducted on the GFP transfected cultures. *Z*-stacks were acquired at higher magnification to facilitate the measurement of spine number, size, and morphology. A ROI, encompassing a segment of 75 μm from the soma of the largest dendrite was defined in one or two of the largest dendrites of the neuron. The bent line overlay tool of LSM Image Examiner 5 was used to measure the length of the spine from the surface of the dendritic shaft, including the neck and head of the spine. The straight-line tool was used to measure the width of the spine at its widest point. Dendritic protrusions were categorized as spines or filopodia, and morphologically classified as mushroom, long, stubby, or thin, using parameters described in ref. 27. Specifically, spines with distinct heads were classified as "mushroom" if less than 2.0 μm in length or "long" if over 2.0 μm in length. Spines without distinct heads were classified as "thin" if less than 2.0 μm in length or "stubby" if less than 1.0 μm in length but wider than 0.35 μm. Protrusions without a distinct head and longer than 2.0 μm were classified as filopodia. The statistical significance of differences in the number, size, and shape of spines across conditions was determined by the Student's *t*-test.

In vivo—*Z*-series stacks were subjected to 3D reconstruction by using Zeiss LSM 510 Meta. Dendritic protrusions were classified as spines (mushroom, long, stubby, or thin) or filopodia as described above, based on the parameters outlined in ref. 27. Size determination of mushroom spines was carried out by using Zeiss LSM image browser overlay tools. The longest straight line in the spine head was counted as the head diameter. The length of the entire spine (including head and stalk) was measured by using a bent-line tool. Differences in the number, size, and shape of spines across conditions were evaluated using the Student's *t*-test. Additional details regarding the analysis of spine numbers and morphology are given in Suppl. Methods.

Electrophysiology

Hippocampal neurons from E17 embryos were plated on microislands (average diameter ≈ 450 μm) of WT, murine, cortical astrocytes. Astrocytes were plated on collagen microdots and allowed to become confluent (4 – 6 days) before neurons were plated on them28,50. Recordings were made after 11 – 14 days in culture from islands containing only a single neuron as described in Suppl. Methods.

Supplementary Material

Refer to Web version on PubMed Central for supplementary material.

ACKNOWLEDGEMENTS

We thank Megan Sirbour, Alexandra Abrams-Downey, Amanda Garçia-Williams and Dionne Swor for technical support and assistance with the mouse colony. We thank Guoping Feng and Peter Scheiffele for constructs. This research was supported in part by NIH (MH67068 to MK and JAG and MH077235 to JAG), a McKnight Brain Disorders Award, an EJLB Scholar award (to JAG) as well as two NARSAD awards (to JAG and JM respectively).

References

1. McDonald-McGinn DM, et al. Phenotype of the 22q11.2 deletion in individuals identified through an affected relative: cast a wide FISHing net! Genetics in Medicine. 2001; 3:23–29. [PubMed: 11339373]
2. Woodin M, et al. Neuropsychological profile of children and adolescents with the 22q11.2 microdeletion. Genetics in Medicine. 2001; 3:34–39. [PubMed: 11339375]
3. Bearden CE, et al. The neurocognitive phenotype of the 22q11.2 deletion syndrome: selective deficit in visual-spatial memory. J. Clin. & Experim. Neuropsychol. 2001; 23:447–464.
4. Sobin C, et al. Neuropsychological characteristics of children with the 22q11 Deletion Syndrome: a descriptive analysis. Child Neuropsychol. 2005; 11:39–53. [PubMed: 15823982]
5. Chow EW, Watson M, Young DA, Bassett AS. Neurocognitive profile in 22q11 deletion syndrome and schizophrenia. Schizophr. Res. 2006; 87:270–278. [PubMed: 16753283]
6. Pulver AE, et al. Psychotic illness in patients diagnosed with velo-cardio-facial syndrome and their relatives. J. Nervous & Mental Dis. 1994; 182:476–478.
7. Karayiorgou M, et al. Schizophrenia susceptibility associated with interstitial deletions of chromosome 22q11. Proc. Natl. Acad. Sci. USA. 1995; 92:7612–7616. [PubMed: 7644464]
8. Xu B, Roos JL, Levy S, van Rensburg EJ, Gogos JA, Karayiorgou M. Strong association of de novo copy number mutations with sporadic schizophrenia. Nat. Genet. 2008; 40:880–885. [PubMed: 18511947]
9. Edelmann L, Pandita RK, Morrow BE. Low-copy repeats mediate the common 3-Mb deletion in patients with velo-cardio-facial syndrome. Am. J. Hum. Genet. 1999; 64:1076–1086. [PubMed: 10090893]
10. Gothelf D, et al. COMT genotype predicts longitudinal cognitive decline and psychosis in 22q11.2 deletion syndrome. Nat. Neurosci. 2005; 8:1500–1502. [PubMed: 16234808]
11. Mukai J, et al. Evidence that the gene encoding ZDHHC8 contributes to the risk of schizophrenia. Nat. Genet. 2004; 36:725–731. [PubMed: 15184899]
12. Paterlini M, et al. Transcriptional and behavioral interaction between 22q11.2 orthologs modulates schizophrenia-related phenotypes in mice. Nat. Neurosci. 2005; 8:1586–1594. [PubMed: 16234811]
13. Raux G, et al. Involvement of hyperprolinemia in cognitive and psychiatric features of the 22q11 deletion syndrome. Hum. Mol. Genet. 2007; 16:83–91. [PubMed: 17135275]
14. Fukata M, Fukata Y, Adesnik H, Nicoll RA, Bredt DS. Identification of PSD95 palmitoylating enzymes. Neuron. 2004; 44:987–996. [PubMed: 15603741]
15. Linder ME, Deschenes RJ. Model organisms lead the way to protein palmitoyltransferases. J. Cell Science. 2004; 117:521–526. [PubMed: 14730009]
16. Roth AF, Feng Y, Chen L, Davis NG. The yeast DHHC cysteine-rich domain protein Akr1p is a palmitoyl transferase. J. Cell Biology. 2002; 159:23–28.
17. Smotrys JE, Linder ME. Palmitoylation of intracellular signaling proteins: regulation and function. Annual Review of Biochem. 2004; 73:559–587.
18. Bijlmakers MJ, Marsh M. The on-off story of protein palmitoylation. Trends in Cell Biology. 2003; 13:32–42. [PubMed: 12480338]
19. el-Husseini Ael D, Bredt DS. Protein palmitoylation: a regulator of neuronal development and function. Nat. Rev. Neurosci. 2002; 3:791–802. [PubMed: 12360323]
20. Chen WY, et al. Case-control study and transmission disequilibrium test provide consistent evidence for association between schizophrenia and genetic variation in the 22q11 gene ZDHHC8. Hum. Mol. Genet. 2004; 13:2991–2995. [PubMed: 15489219]
21. Glaser B, et al. No association between the putative functional ZDHHC8 single nucleotide polymorphism rs175174 and schizophrenia in large European samples. Biol. Psychiatry. 2005; 58:78–80. [PubMed: 15992527]
22. Puech A, et al. Comparative mapping of the human 22q11 chromosomal region and the orthologous region in mice reveals complex changes in gene organization. Proc. Natl. Acad. Sci. USA. 1997; 94:14608–14613. [PubMed: 9405660]

23. Stark KL, et al. Altered brain microRNA biogenesis contributes to phenotypic deficits in a 22q11-deletion mouse model. Nat. Genet. 2008; 40:751–760. [PubMed: 18469815]
24. El-Husseini AE, Schnell E, Chetkovich DM, Nicoll RA, Bredt DS. PSD95 involvement in maturation of excitatory synapses. Science. 2000; 290:1364–1368. [PubMed: 11082065]
25. Sala C, et al. Regulation of dendritic spine morphology and synaptic function by Shank and Homer. Neuron. 2001; 31:115–130. [PubMed: 11498055]
26. Charych EI, et al. Activity-independent regulation of dendrite patterning by postsynaptic density protein PSD95. J. Neurosci. 2006; 26:10164–10176. [PubMed: 17021172]
27. Chakravarthy S, et al. Postsynaptic TrkB signaling has distinct roles in spine maintenance in adult visual cortex and hippocampus. Proc. Natl. Acad. Sci. USA. 2006; 103:1071–1076. [PubMed: 16418274]
28. Bekkers JM, Stevens CF. Excitatory and inhibitory autaptic currents in isolated hippocampal neurons maintained in cell culture. Proc. Natl. Acad. Sci. USA. 1991; 88:7834–7838. [PubMed: 1679238]
29. Cho KO, Hunt CA, Kennedy MB. The rat brain postsynaptic density fraction contains a homolog of the Drosophila discs-large tumor suppressor protein. Neuron. 1992; 9:929–942. [PubMed: 1419001]
30. Kornau HC, Schenker LT, Kennedy MB, Seeburg PH. Domain interaction between NMDA receptor subunits and the postsynaptic density protein PSD95. Science. 1995; 269:1737–1740. [PubMed: 7569905]
31. Bellocchio EE, Reimer RJ, Fremeau RT Jr, Edwards RH. Uptake of glutamate into synaptic vesicles by an inorganic phosphate transporter. Science. 2000; 289:957–960. [PubMed: 10938000]
32. Ohno Y, Kihara A, Sano T, Igarashi Y. Intracellular localization and tissue-specific distribution of human and yeast DHHC cysteine-rich domain-containing proteins. Biochim. Biophys. Acta. 2006; 1761:474–483. [PubMed: 16647879]
33. Gauthier-Campbell C, Bredt DS, Murphy TH, El-Husseini Ael D. Regulation of dendritic branching and filopodia formation in hippocampal neurons by specific acylated protein motifs. Mol. Biol. Cell. 2004; 15:2205–2217. [PubMed: 14978216]
34. Feng G, et al. Imaging neuronal subsets in transgenic mice expressing multiple spectral variants of GFP. Neuron. 2000; 28:41–51. [PubMed: 11086982]
35. Tada T, Sheng M. Molecular mechanisms of dendritic spine morphogenesis. Curr. Opin. Neurobiol. 2006; 16:95–101. [PubMed: 16361095]
36. Vessey JP, Karra D. More than just synaptic building blocks: scaffolding proteins of the post-synaptic density regulate dendritic patterning. J. Neurochem. 2007; 102:324–332. [PubMed: 17596209]
37. El-Husseini Ael D, et al. Synaptic strength regulated by palmitate cycling on PSD95. Cell. 2002; 108:849–863. [PubMed: 11955437]
38. Topinka JR, Bredt DS. N-terminal palmitoylation of PSD95 regulates association with cell membranes and interaction with K+ channel Kv1.4. Neuron. 1998; 20:125–134. [PubMed: 9459448]
39. Ehrlich I, Klein M, Rumpel S, Malinow R. PSD95 is required for activity-driven synapse stabilization. Proc. Natl. Acad. Sci. USA. 2007; 104:4176–4181. [PubMed: 17360496]
40. Firestein BL, Craven SE, Bredt DS. Postsynaptic targeting of MAGUKs mediated by distinct N-terminal domains. Neuroreport. 2000; 11:3479–3484. [PubMed: 11095503]
41. Kanaani J, Diacovo MJ, El-Husseini Ael D, Bredt DS, Baekkeskov S. Palmitoylation controls trafficking of GAD65 from Golgi membranes to axon-specific endosomes and a Rab5a-dependent pathway to presynaptic clusters. J. Cell Science. 2004; 117:2001–2013. [PubMed: 15039456]
42. Kang R, et al. Presynaptic trafficking of synaptotagmin I is regulated by protein palmitoylation. J. Biol. Chem. 2004; 279:50524–50536. [PubMed: 15355980]
43. Washbourne P, et al. Cysteine residues of SNAP-25 are required for SNARE disassembly and exocytosis, but not for membrane targeting. Biochem. J. 2001; 357:625–634. [PubMed: 11463334]
44. Berthiaume L, Resh MD. Biochemical characterization of a palmitoyl acyltransferase activity that palmitoylates myristoylated proteins. J. Biol. Chem. 1995; 270:22399–22405. [PubMed: 7673226]

45. El-Husseini AE, et al. Dual palmitoylation of PSD95 mediates its vesiculotubular sorting, postsynaptic targeting, and ion channel clustering. J. Cell Biol. 2000; 148:159–172. [PubMed: 10629226]

46. Karayiorgou M, Gogos JA. The molecular genetics of the 22q11-associated schizophrenia. Mol. Brain Res. 2004; 132:95–104. [PubMed: 15582150]

47. Valdez-Taubas J, Pelham H. Swf1-dependent palmitoylation of the SNARE Tlg1 prevents its ubiquitination and degradation. EMBO J. 2005; 24:2524–2532. [PubMed: 15973437]

48. Huang K, et al. Huntingtin-interacting protein HIP14 is a palmitoyl transferase involved in palmitoylation and trafficking of multiple neuronal proteins. Neuron. 2004; 44:977–986. [PubMed: 15603740]

49. Arguello PA, Gogos JA. Modeling madness in mice: one piece at a time. Neuron. 2006; 52:179–196. [PubMed: 17015235]

50. Gu JG, MacDermott AB. Activation of ATP P2X receptors elicits glutamate release from sensory neuron synapses. Nature. 1997; 389:749–753. [PubMed: 9338789]

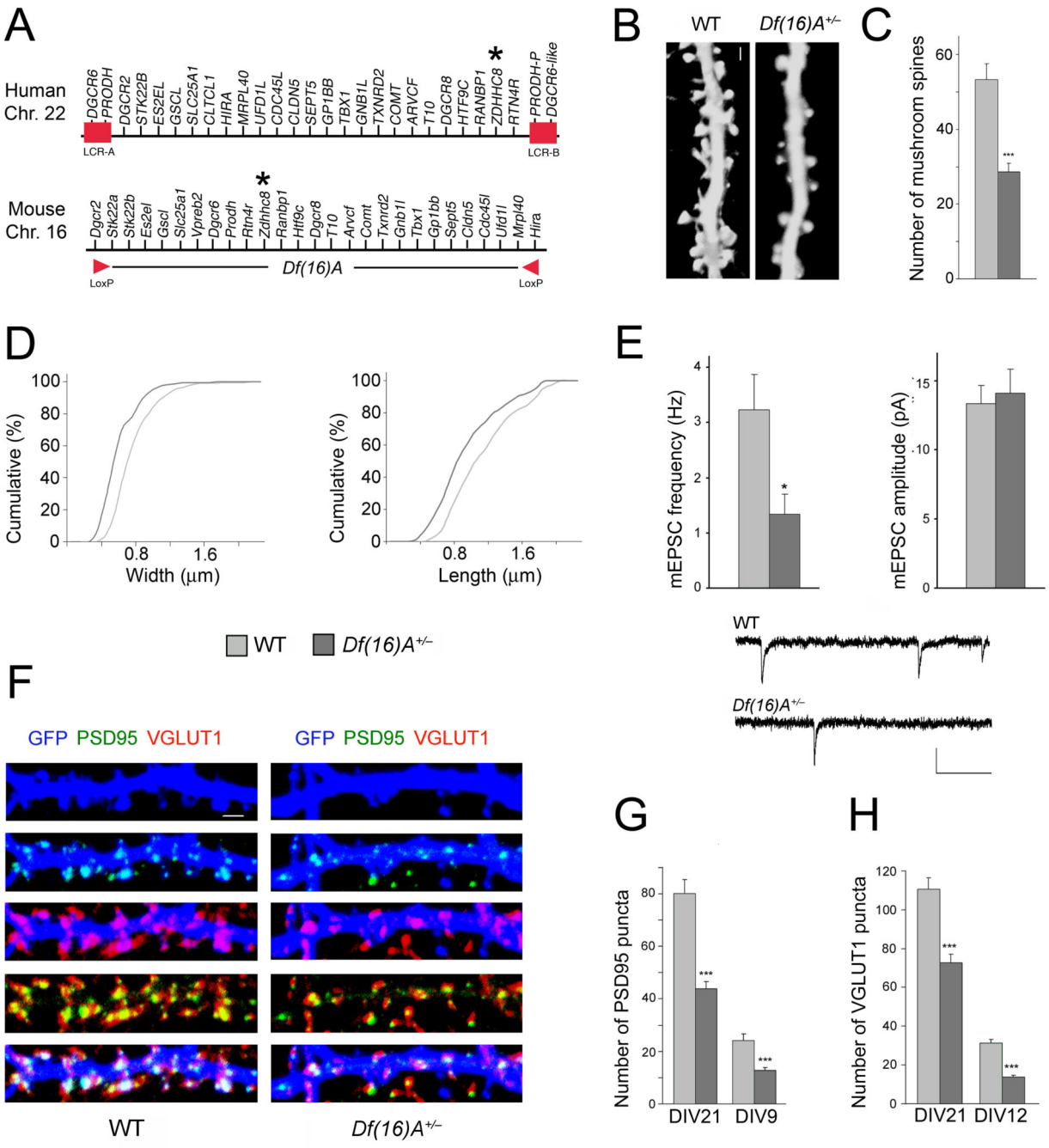

Figure 1. *Df(16)A*$^{+/-}$ neurons show reduced density of spines and glutamatergic synapses

(**a**) Schematic showing the human 22q11.2 region and the syntenic mouse region. The 1.5-Mb deletion found in patients is mediated by low copy repeat sequences LCR-A and LCR-B (red boxes). *Dgcr2* and *Hira*, the two endpoints of the targeted deletion where loxP sites were inserted23, are indicated by red arrowheads. The location of the human and mouse *ZDHHC8* gene is indicated by an asterisk.

(**b**) Representative images of spines in *Df(16)A*$^{+/-}$ neurons (DIV21) transfected with a EGFP, which fills and clearly defines dendritic protrusions. Scale bar, 1 µm.

(**c**) Reductions in the number of mushroom spines observed at DIV21 on *Df(16)A*$^{+/-}$ neurons (estimated over 75 μm of dendritic length).
(**d**) Reductions in the width (*left*) and length (*right*) of mushroom spines on *Df(16)A*$^{+/-}$ neurons. $P < 0.05$, K-S test.
(**e**) Properties of mEPSC recorded from autaptic individual pyramidal neurons grown on astrocytic microislands. *Top left*: the frequency at which events occurred was lower in *Df(16)A*$^{+/-}$ neurons ($n = 10$) than in WT controls ($n = 11$). *Top right:* The average amplitude of mEPSCs was not different between genotypes. *Bottom:* Traces of recordings from a WT and a *Df(16)A*$^{+/-}$ neuron. Scale bars, vertical: 20 pA, horizontal: 100 msec.
(**f**) Representative images of PSD95 puncta (*green*) and VGLUT1 puncta (*red*) and their co-localization in GFP (*blue*)-labeled hippocampal neurons at DIV21. Scale bar, 1 μm.
(**g**) Reduction in the number of PSD95 puncta in *Df(16)A*$^{+/-}$ neurons at DIV21 and DIV9.
(**h**) Reduction in the number of VGLUT1 puncta in *Df(16)A*$^{+/-}$ neurons at DIV21 and DIV12. Data are shown as mean ± S.E.M. * $P < 0.05$, *** $P < 0.0001$.

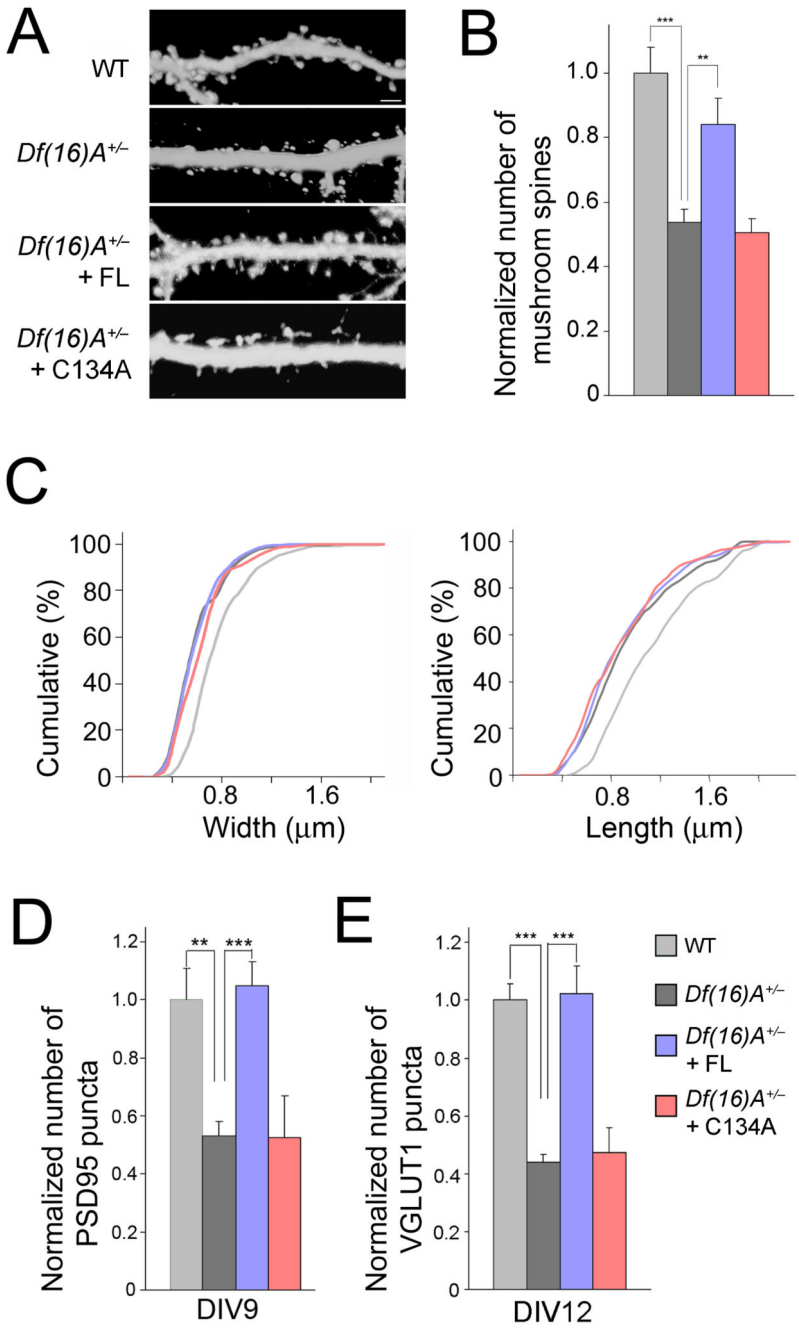

Figure 2. Enzymatically active ZDHHC8 protein prevents deficits

(**a**) Representative images of spines in *Df(16)A*$^{+/-}$ neurons (DIV21) transfected with a plasmid expressing EGFP. Scale bar, 2 μm.

(**b**) Transfection of *ZDHHC8-FL* (but not of *-C134A*) restores spine number density to WT levels in *Df(16)A*$^{+/-}$ neurons.

(**c**) Transfection of active *ZDHHC8-FL* or *-C134A* does not influence the length or width of mushroom spines of *Df(16)A*$^{+/-}$ neurons. $P > 0.05$, K-S test.

(**d,e**) The reduction in the puncta number of PSD95 at DIV9 (**d**), VGLUT1 at DIV12 (**e**), in *Df(16)A*$^{+/-}$ neurons is reversed upon introduction of *ZDHHC8-FL*, but not -*C134A*. Bar graphs shows puncta density normalized to WT (first bar). Data are shown as mean ± S.E.M. ** $P < 0.001$, *** $P < 0.0001$.

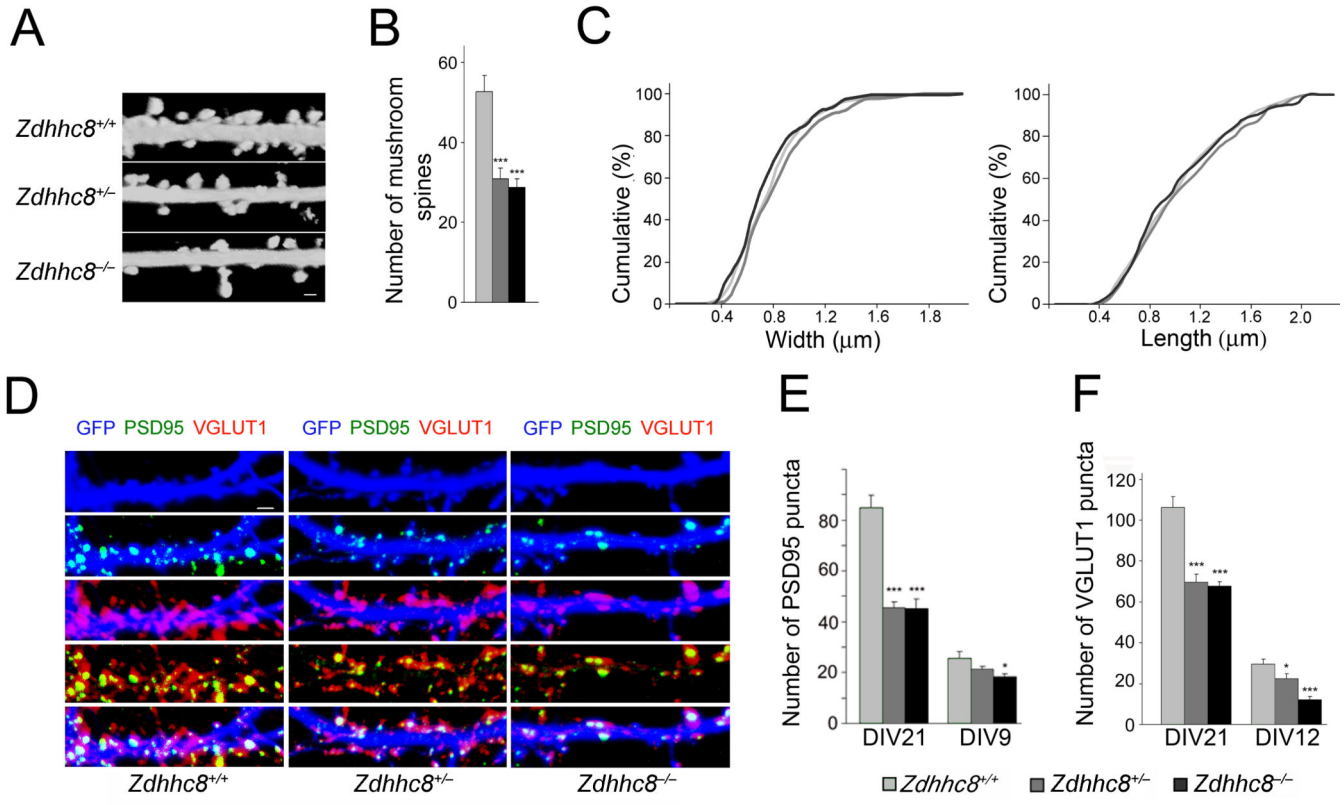

Figure 3. Zdhhc8-deficiency affects the density of spines and glutamatergic synapses

(**a**) Representative images of spines in DIV21 *Zdhhc8*-deficient neurons transfected with a plasmid expressing EGFP. Scale bar, 1 μm.

(**b**) Reduction in the number of mushroom spines (estimated over 75 μm of dendritic length) in $Zdhhc8^{+/-}$ and $Zdhhc8^{-/-}$ neurons.

(**c**) No differences are observed in the width (*left*) or length (*right*) of mushroom spines in $Zdhhc8^{+/-}$ or $Zdhhc8^{-/-}$ neurons relative to WT neurons. $P > 0.05$, K-S test.

(**d**) PSD95 (*green*) and VGLUT1 puncta (*red*) and their co-localization in GFP (*blue*)-labeled WT or *Zdhhc8*-deficient neurons at DIV21. Scale bar, 1 μm.

(**e**) Reduced PSD95 puncta number (per 50 μm of dendritic length) at DIV21 and DIV9 in *Zdhhc8*-deficient neurons.

(**f**) Reduced VGLUT1 puncta number at DIV21 and DIV12 in *Zdhhc8*-deficient neurons.

Data are shown as mean ± S.E.M. * $P < 0.05$, *** $P < 0.0001$.

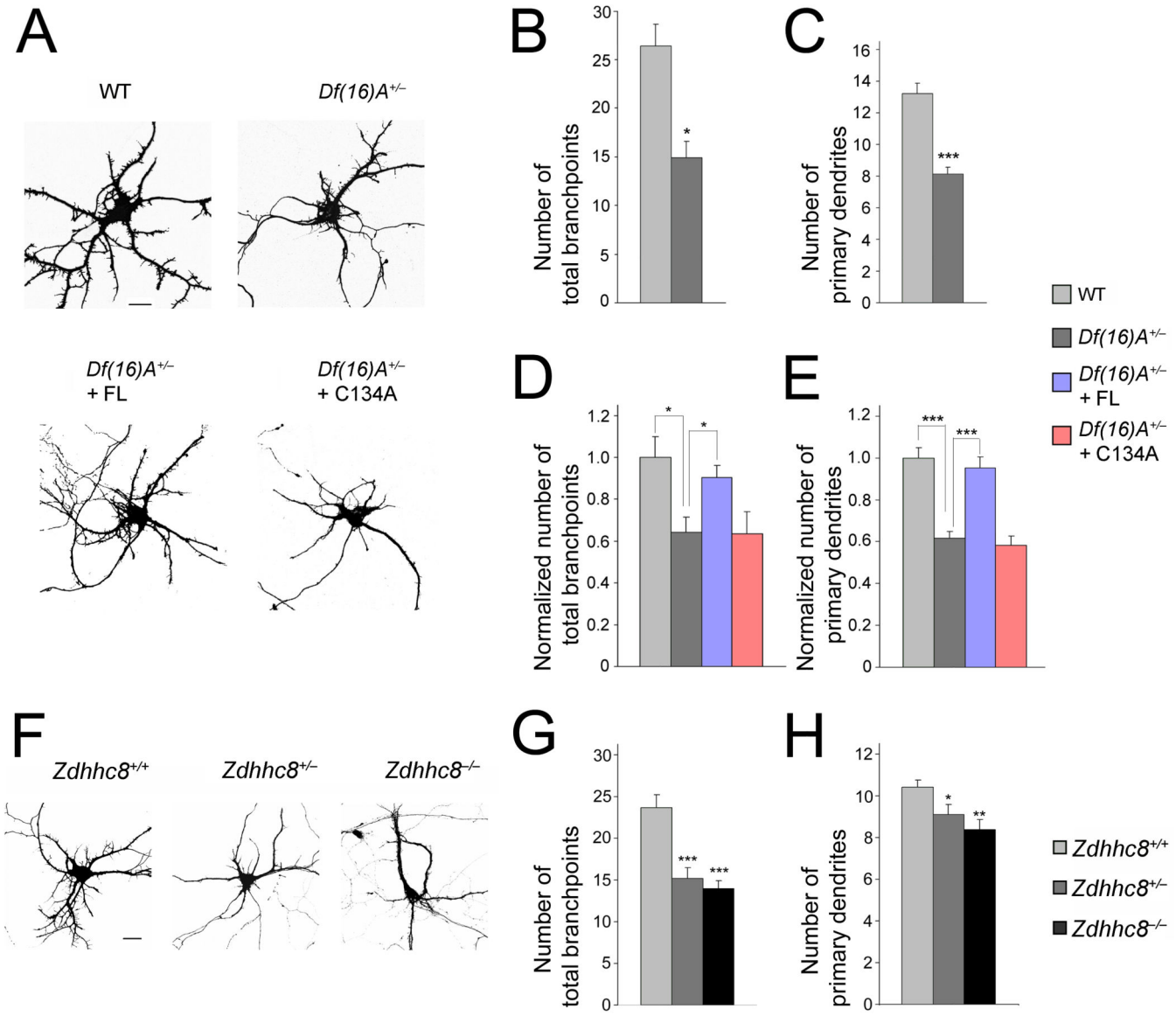

Figure 4. ZDHHC8-dependent reduction in dendritic complexity in *Df(16)A*$^{+/-}$ neurons

(**a**) *Df(16)A*$^{+/-}$ neurons transfected with EGFP at DIV9. Scale bar, 20 μm.

(**b,c**) Reduction in the number of branchpoints (**b**) and number of primary dendrites emanating from the soma (**c**) in *Df(16)A*$^{+/-}$ neurons.

(**d,e**) Reduction in the number of branchpoints (**d**) and number of primary dendrites (**e**) in *Df(16)A*$^{+/-}$ neurons is prevented by transfection of *ZDHHC8-FL* (but not of *-C134A*) into *Df(16)A*$^{+/-}$ neurons. Bar graphs shows puncta density normalized to WT (first bar).

(**f**) Representative images of *Zdhhc8*-deficient neurons at DIV9, transfected with a plasmid expressing EGFP. Scale bar, 20 μm.

(**g,h**) Reduction in the number of branchpoints (**g**) and number of primary dendrites emanating from the soma (**h**) in *Zdhhc8*$^{+/-}$ and *Zdhhc8*$^{-/-}$ neurons. Data are shown as mean ± S.E.M. * $P < 0.05$, ** $P < 0.001$, *** $P < 0.0001$.

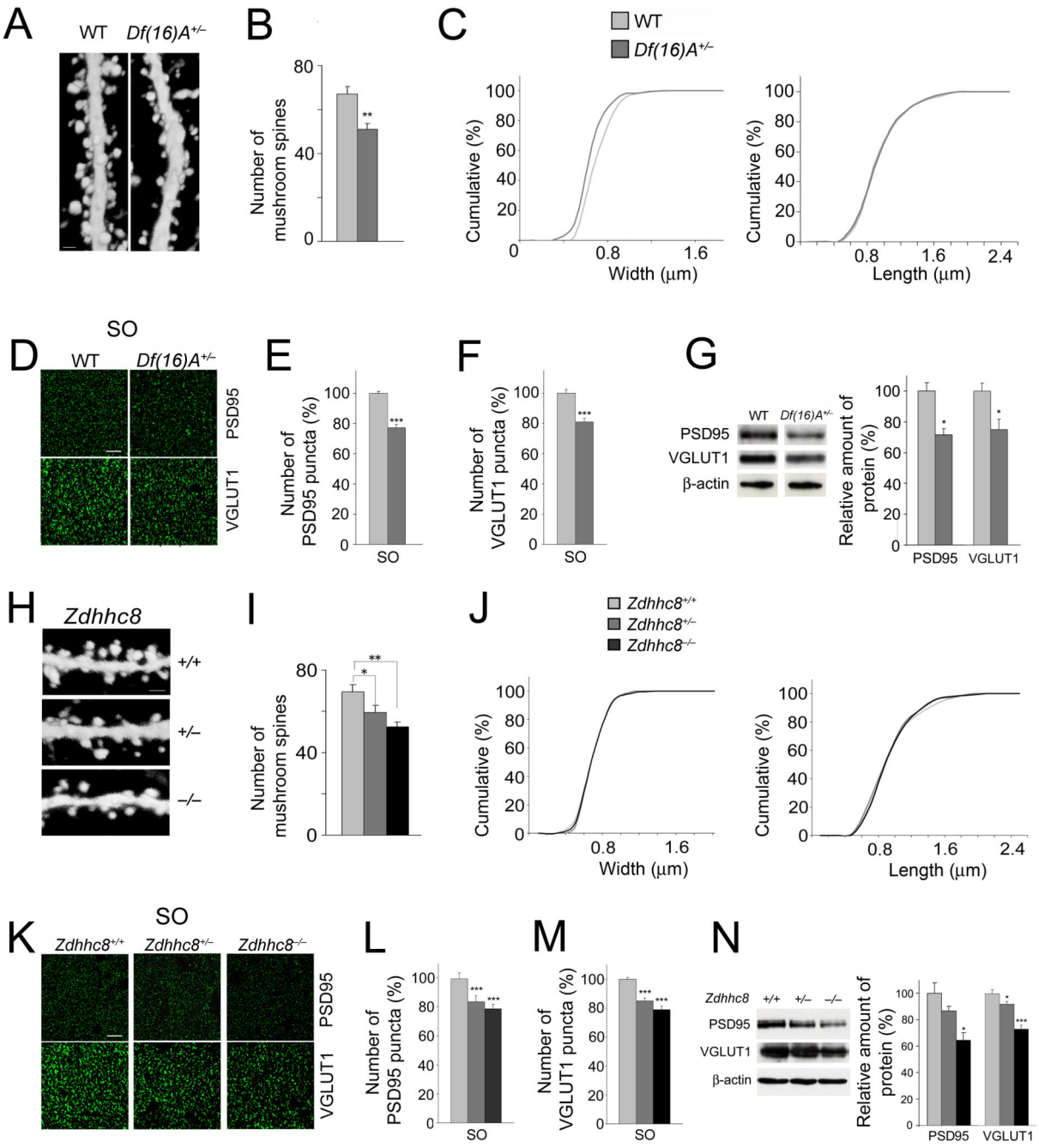

Figure 5. Alterations in spines/excitatory synapses in the HPC of mutant mice

(**a**) High magnification representative images of EGFP-expressing neurons in the CA1 region of the HPC of *Thy1-GFP*$^{+/-}$ (*left*) and *Df(16)A*$^{+/-}$*;Thy1-GFP*$^{+/-}$ (*right*) mice. Dendritic spines located at basal dendrites are shown. Scale bar, 1 μm.

(**b**) The density of mushroom spines (estimated over 75 μm of dendritic length) is reduced in *Df(16)A*$^{+/-}$*;Thy1-GFP*$^{+/-}$ neurons.

(**c**) Reduction in the width (*left*: $P < 0.05$, K-S test), but not length (*right*: $P > 0.05$, K-S test), of mushroom spines of *Df(16)A*$^{+/-}$*;Thy1-GFP*$^{+/-}$ CA1 hippocampal neurons relative to WT *Thy1-GFP*$^{+/-}$ CA1 neurons.

(**d**) Representative images of the immunohistochemical analysis for PSD95 (*top*) and VGLUT1 (*bottom*) puncta performed on hippocampal slices from adult *Df(16)A*$^{+/-}$ mice and WT littermates. Scale bar, 10 μm.

(**e,f**) Quantification of PSD95 (**e**) and VGLUT1 (**f**) puncta number in the SO layer sampled along the dorsal/ventral axis of the HPC in the *Df(16)A*$^{+/-}$ mice.

(**g**) Total protein levels of PSD95 and VGLUT1 in HPC lysates from adult *Df(16)A*$^{+/-}$ mice and WT littermates. Representative western blot images are shown on the left.

(**h**) Representative images of CA1 EGFP-expressing neurons from the HPC of *Zdhhc8*$^{+/+}$*;Thy1-GFP*$^{+/-}$ (*top*), *Zdhhc8*$^{+/-}$*;Thy1-GFP*$^{+/-}$ (*center*) and *Zdhhc8*$^{-/-}$*;Thy1-GFP*$^{+/-}$ (*bottom*) mice. Spines located on basal dendrites are shown. Scale bar, 1 μm.

(**i**) The density of mushroom spines (estimated over 75 μm of dendritic length) is reduced in *Zdhhc8*$^{+/-}$*;Thy1-GFP*$^{+/-}$ and *Zdhhc8*$^{-/-}$*;Thy1-GFP*$^{+/-}$ neurons.

(**j**) No differences are observed in the width (*left*: $P > 0.05$, K-S test) or length (*right*: $P > 0.05$, K-S test) of mushroom spines in *Zdhhc8*$^{+/-}$ or *Zdhhc8*$^{-/-}$ neurons.

(**k**) Representative images of the immunohistochemical analysis for PSD95 (*top*) and VGLUT1 (*bottom*) puncta performed on hippocampal slices from adult *Zdhhc8*$^{+/-}$ and *Zdhhc8*$^{-/-}$ mice and WT littermates. Scale bar, 10 μm.

(**l,m**) PSD95 (**l**) and VGLUT1 (**m**) puncta numbers in the SO layer, sampled along the dorsal/ventral axis of the HPC of adult *Zdhhc8*$^{+/-}$ or *Zdhhc8*$^{-/-}$ mice and WT littermates.

(**n**) Western blot analysis of total protein levels of PSD95 and VGLUT-1 in HPC lysates from adult *Zdhhc8*$^{+/-}$ and *Zdhhc8*$^{-/-}$ mice and WT littermates. Representative images are shown on the left. Data are shown as mean ± S.E.M. * $P < 0.05$, ** $P < 0.001$, *** $P < 0.0001$.

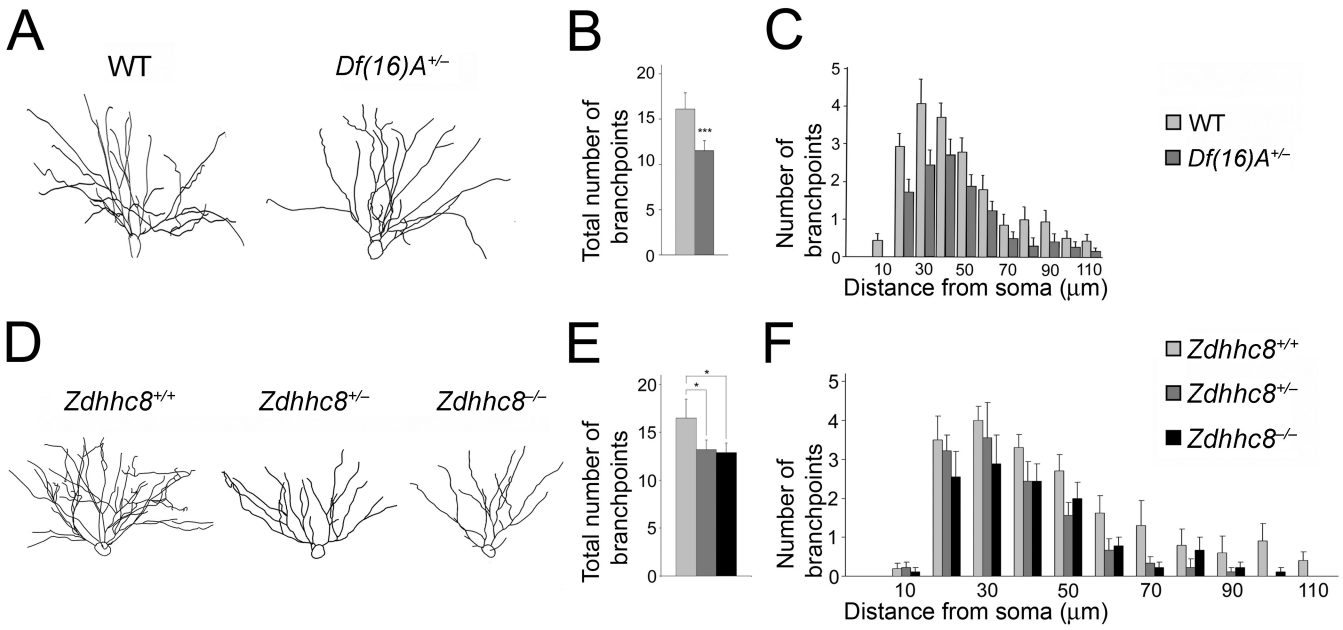

Figure 6. Alterations in dendritic complexity in the HPC of mutant mice

(**a**) Representative tracings of the basal dendritic tree of pyramidal neurons from the CA1 region of the HPC of *Df(16)A*$^{+/-}$*;Thy1-GFP*$^{+/-}$ and WT *Thy1-GFP*$^{+/-}$ mice.

(**b**) Reduction in the total number of branchpoints of basal dendrites in *Df(16)A*$^{+/-}$*;Thy1-GFP*$^{+/-}$ CA1 hippocampal neurons relative to WT *Thy1-GFP*$^{+/-}$ CA1 neurons.

(**c**) Sholl analysis of dendritic complexity using 10 μm concentric circles around the soma. A repeated measures ANOVA examining the interaction between branchpoints and distance from the soma shows an overall genotype effect indicating a significant reduction in branching prevalent throughout the dendritic tree ($n = 18$, $P < 0.008$).

(**d**) Representative tracings of the basal dendritic tree of pyramidal neurons from the CA1 region of the HPC of *Zdhhc8*$^{+/+}$*;Thy1-GFP+/–, Zdhhc8+/–;Thy1-GFP*$^{+/-}$ and *Zdhhc8*$^{-/-}$ *;Thy1-GFP*$^{+/-}$ mice.

(**e**) Reduction in the total number of branchpoints of basal dendrites in *Zdhhc8*$^{+/-}$*;Thy1-GFP*$^{+/-}$ and *Zdhhc8*$^{-/-}$*;Thy1-GFP*$^{+/-}$ CA1 hippocampal neurons.

(**f**) Sholl analysis of dendritic complexity. Analysis of the interaction between branchpoints and distance from the soma shows an overall genotype effect ($n = 36$, $P < 0.01$). Data are shown as mean ± S.E.M. * $P < 0.05$, ** $P < 0.001$, *** $P < 0.0001$.

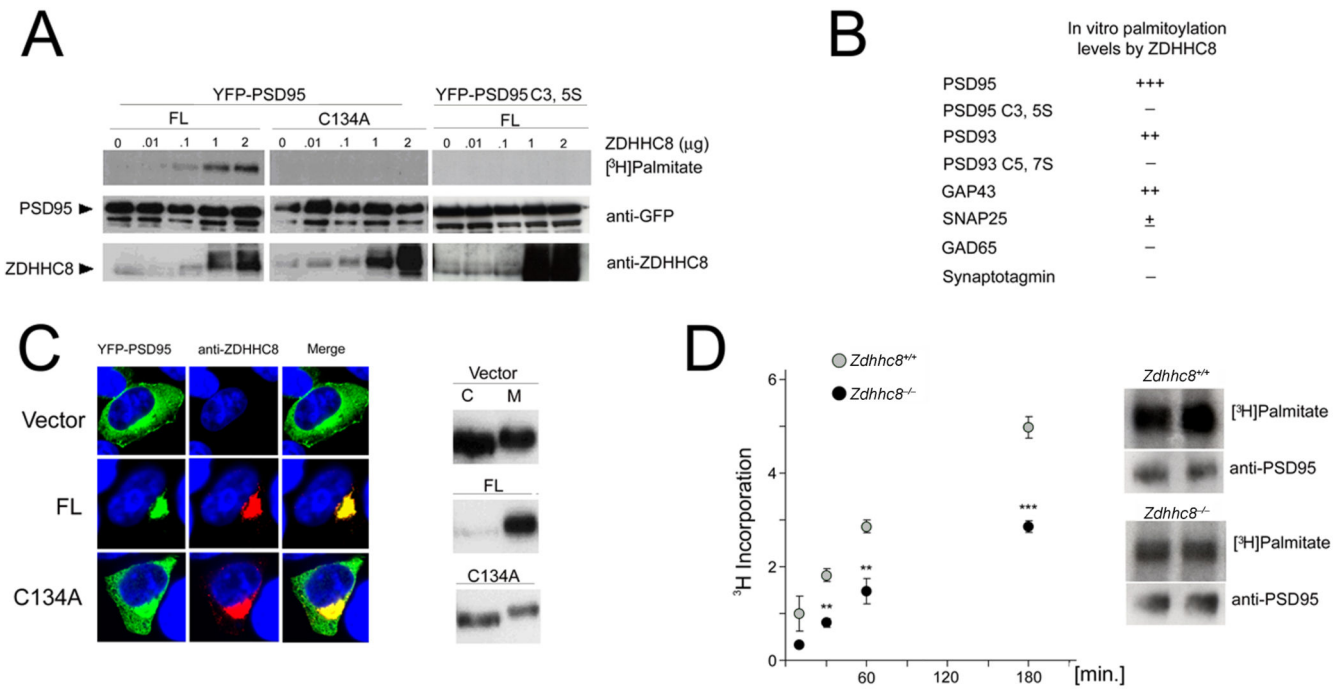

Figure 7. ZDHHC8 shows PAT activity toward PSD95

(**a**) ZDHHC8 activity increases the amount of palmitate incorporated into PSD95 in HEK293 cells. HEK293 cells were transiently transfected with *YFP-PSD95* or *YFPPSD95 C3,5S* and *ZDHHC8-FL* or *-C134A*. YFP-PSD95 (but not YFP-PSD95 C3,5S) was palmitoylated by *ZDHHC8-FL* (but not *-C134A*) in a dose dependent manner.

(**b**) In addition to PSD95, ZDHHC8 increased incorporation of palmitate in PSD93, as well as GAP43. There was very little, if any, ZDHHC8-dependent incorporation of palmitate in SNAP25, GAD65, or Synaptotagmin-1 in HEK293 cells.

(**c**) *Left:* The effect of ZDHHC8 on PSD95 distribution in HEK293 cells. YFP-PSD95 was co-expressed with *ZDHHC8-FL* into HEK293 cells. *ZDHHC8-FL* but not *-C134A* specifically increases the accumulation of WT PSD95 at the perinuclear region. *Right:* Sub-fractionation of PSD95 in the presence or absence of ZDHHC8 in HEK293 cells. The distribution of PSD95 into Triton X-100-soluble (*C*) and Triton X-100-insoluble (*M*) fractions was analyzed by western blotting with a PSD95 antibody.

(**d**) Palmitate incorporation into endogenous PSD95 is compromised in *Zdhhc8*-deficient neurons at DIV21. *Left:* Graph indicating levels of palmitoylated PSD95 in *Zdhhc8*$^{-/-}$ cultures compared to WT cultures (t = 10, 30, 60, 180 minutes: *n* = 3, 6, 6, 11, respectively, at each time point). *Right:* Representative fluorographs and immunoblots of PSD95 at 180 min following incubation with [^{3}H] palmitate.